# Application of Aerial InSAR to Measure Glacier Elevations

**Bryce Glenn[1], Andrew G. Fountain[1], Delwyn Moller[2]**

[1] Department of Geology, Portland State University, Portland, Oregon, USA 97207

[2] Department of Electrical, Computer & Software Engineering, University of Auckland, Auckland, New Zealand

Corresponding author: Andrew G. Fountain, andrew@pdx.edu

**Key Points:**

- Aerial InSAR can rapidly map the topography of alpine glaciers over a broad region.
- Elevations compare favorably to lidar, +0.17 ± 1.78 m at spatial scale of 3 m.
- The mean rate of glacier elevation change (specific volume) is -0.3 ± 0.2 m $yr^{-1}$ for the past 56 years with rates increasing since 1980.

## Abstract

Glaciers and perennial snowfields are important to alpine ecosystems and regional hydrology. Quantifying volume change of a population of glaciers widely distributed over a region is difficult and expensive. We employed NASA's novel Airborne Glacier and Ice Surface Topography Interferometer (GLISTIN) to rapidly map surface topography of alpine glaciers across the western USA. In five flight days 3289 glaciers and perennial snowfields were surveyed. Comparison with lidar over control sites showed a mean difference of +0.17 ±1.78 m at a spatial scale of 3 m. Data coverage increased and elevation uncertainty decreased with the mosaicking of multiple passes due to the complex terrain. Elevation change since the National Elevation Dataset shows a thinning (and volume loss) over the last ~56 years, averaging -0.3 ± 0.2 m and accelerating since 1980. GLISTIN can be a valuable tool for rapidly mapping ice surfaces in the alpine environment.

## Plain Language Summary

Glaciers and perennial snowfields are important water sources to alpine ecosystems and regional hydrology. To quantify their contribution their volume change is measured by mapping elevation changes of the ice surface. However, quantifying volume change for a population of glaciers widely distributed over a region is difficult and expensive. We employed NASA's airborne radar (GLISTIN) to rapidly map surface topography of alpine glaciers across the western USA. In only five flight days 3289 glaciers and perennial snowfields were surveyed. GLISTIN data over control-regions were compared to lidar, an independent elevation measure using lasers, and showed small differences indicating this method can be a valuable and cost-effective tool to track glacier change in the future. Comparing the new elevations against historic elevations from USGS maps a dramatic thinning (and volume loss) over the last ~60 years.

## 1. **Introduction**

Glacier melt is important to runoff in high alpine landscapes. At a local scale, melting glaciers maintain streamflow during the dry, late summer months after the seasonal snow has melted (Fountain & Tangborn, 1985; Moore et al., 2009). Shrinking glaciers lose ice volume and supply more water to streams and rivers than anticipated from precipitation. Although this may be a temporary benefit, particularly in dry regions, their ability to buffer seasonal runoff in future is reduced, making watersheds more vulnerable to drought (Hall & Fagre, 2003; Moore et al., 2009). At a global scale, mass transfer of water from storage as ice to water runoff increases global sea-levels (Meier, 1984; Pfeffer et al., 2014; Zemp et al., 2019).

Traditionally, tracking glacier mass change was a field effort based on measuring the gain and loss of snow and ice at points on the glacier (Kaser et al., 2003; Ostrem & Brugman, 1991). Although these efforts produce high-quality results showing spatial variations in mass change across a glacier only a few glaciers can be so monitored by any agency (Andreassen et al., 2005; O'Neel et al., 2019). Remote-sensing methods can be used to cover broad regions using an alternative approach that estimates mass change from volume change. Differential interferometric synthetic aperture radar (InSAR) can map surface elevation changes and offers the advantage of an all-weather, day/night capability, a particularly valuable tool in often cloudy alpine environments (Rosen et al., 2000). Satellite-borne applications have revolutionized our understanding of Antarctica and Greenland (Mouginot et al., 2019; Shepherd et al., 2018), and more recently, the larger alpine glaciers (Millan et al., 2022). Challenges using InSAR include shadowing, decorrelation due to layover, phase unwrapping, and temporal landscape changes (Eineder & Holzner, 2000; Rees, 2000).

Here, we test a novel approach for determining surface elevations on alpine glaciers using an airborne single-pass InSAR, NASA's Glacier, and Ice Surface Topography Interferometer (GLISTIN; Moller et al., 2017). Unlike differential/repeat-pass InSAR, GLISTIN collects two radar images simultaneously, allowing elevations to be derived from a single flight pass and are thus not sensitive to temporal decorrelation between observations. Mounted on a jet aircraft, GLISTIN can image large areas in a short time and has been used to map the relatively gentle topography of large glaciers and ice sheets

(Hensley et al., 2016; Moller et al., 2019). We evaluate its performance to map small alpine glaciers in complex terrain across a broad region. In addition, the updated glacier elevations are differenced from the National Elevation Data (Gesch, 2002) to calculate glacier elevation change across the western US.

## 2. Data and Methods

### 2.1 Study Area

The study region is the American West, defined as the continental United States west of the 100th meridian enclosing about $2x10^6$ $km^2$ and home to about 5036 glaciers and perennial snowfields (≥0.01 $km^2$) as of the late 20th century (Figure 1; Fountain et al., 2017). The region is made up of three large mountain ranges, the Rocky Mountains, the Cascade Range, and the Sierra Nevada. Many peaks exceed 4000 m in. The largest concentration of glaciers, and lowest elevation (2000 m - 3000 m asl) is in the maritime climate of the Pacific Northwest (Oregon, Washington, north-west Montana,). The remaining glaciers are in continental climates elsewhere at high elevations, > 3000m.

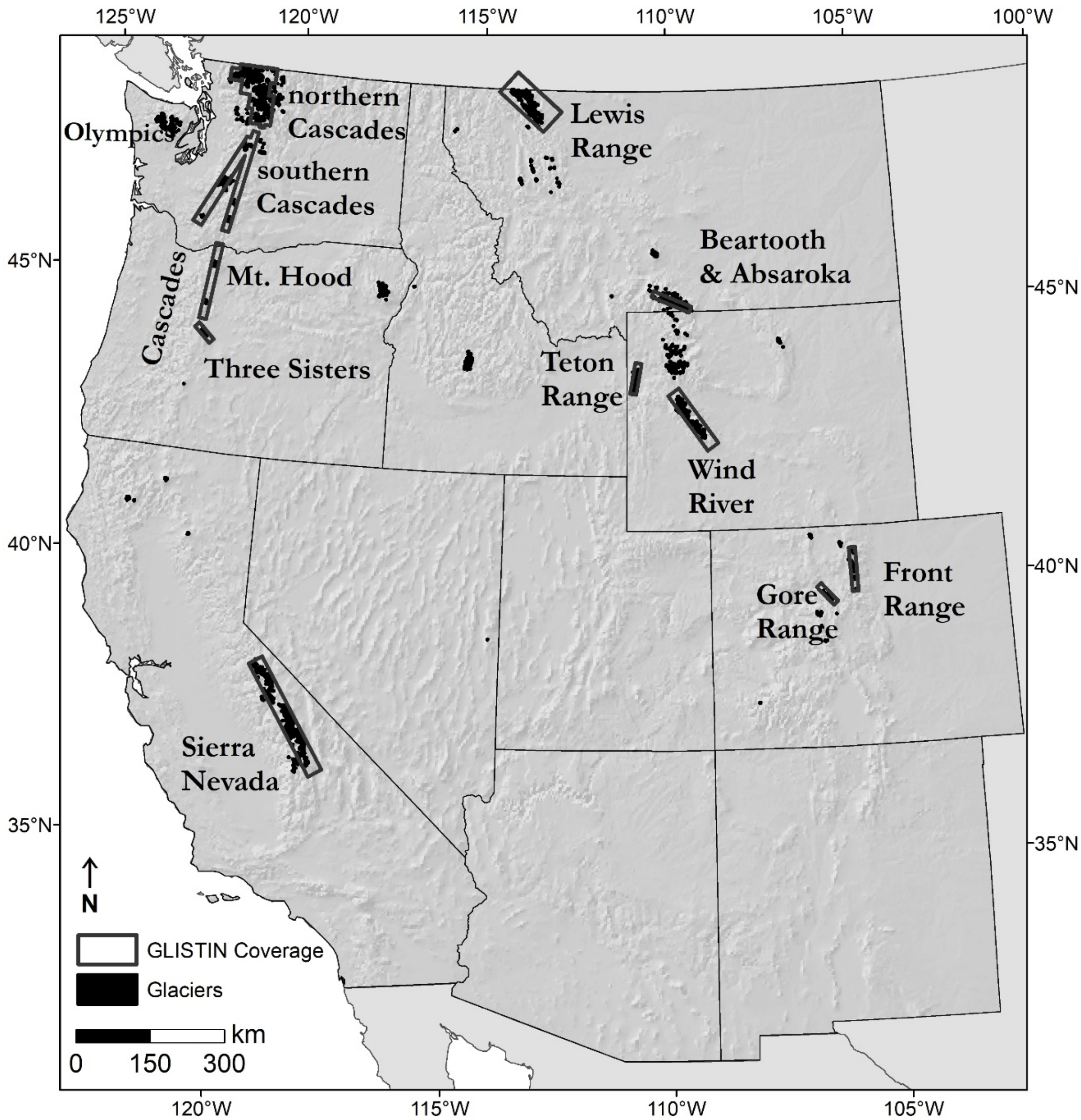


**Figure 1.** Map of glaciers and perennial snowfields (black dots) in the Western U.S. The boxes show regions surveyed by GLISTIN.

Regional studies have shown drastic decreases in glacier area exceeding 50% over the last century (DeVisser & Fountain, 2015; Fagre et al., 2017; O'Neel et al., 2019). The rate of change has not been constant or spatially uniform (Basagic & Fountain, 2011; Hoffman et al., 2007; O'Neal et al., 2015). Glacier volume changes, estimated by differencing topography over time, show a loss on Mount Rainier, WA, of -0.65 $km^3$, average specific mass loss rate of -0.16 m w.e $yr^{-1}$ (1970 - 2007/2008; Sisson et al., 2011). Menounos et al. (2018) estimated a volume loss of -127.65 ± 45.17 $km^3$, -0.42 ± 0.15 m w.e. between 2000 and 2018 for most of the glaciated terrain in Western North America.

## 2.2 GLISTIN

GLISTIN is a Ka-band radar (8.4 mm, 35.66 GHz) system that utilizes two horizontally polarized antennas, 0.25 m apart in elevation, both of which are capable of transmitting and receiving (Moller et al., 2019). Unlike repeat-pass InSAR, GLISTIN's dual antennas, collect data simultaneously. The Ka-band center frequency enables high accuracy with a compact architecture and reduces snow penetration compared to lower frequencies. This cross-track InSAR system is capable of providing not only the position of each image point in along-track and slant range as with traditional SAR but also the height of that point via the interferometric phase. Because the phase repeats after $2\pi$, it must be "unwrapped" to determine its unique location and height relative to a reference surface (Moller et al., 2011; Rosen et al., 2000). The system is contained in an external pod beneath NASA's Gulfstream-III aircraft with left looking view angles of 15-50° from nadir. The system is coupled to inertial navigation and global position that provide pitch and roll of the aircraft as well as its precise position in space. Nominal flight altitudes are about 12,500 m above sea-level with a ground swath width of about 12 km and its typical air speed is 720 km $hr^{-1}$.

To guide the aerial survey, the locations of the glaciers were retrieved from Fountain et al. (2017). Flight passes were typically flown in pairs, each in an opposite direction, to reduce gaps in backscatter from radar shadow or layover in the mountainous terrain. In a few regions additional perpendicular flight passes were also flown. The georectified height-maps from each pass were mosaicked into a 3-meter pixel-size digital elevation model (DEM; Hensley et al., 2016) and projected into the Universal Transverse Mercator (UTM) coordinate system. Self-reported elevation accuracy is 'height-precision', a statistical estimate based on the interferometric correlation of each individual radar pixel making up the 3 m mosaicked pixel (Moller et al., 2011). In the final mosaicked DEM, the elevation of each pixel is the weighted sum of elevations from individual passes and the weights are inversely proportional to the height-precision (Hensley et al., 2016). The vertical absolute uncertainty of GLISTIN-derived topography was found to be about ± 0.30 m over bare non-snow-covered terrain (Schumann et al., 2016). Data collection and processing were provided by the Jet Propulsion Laboratory at California Institute of Technology, Pasadena, CA.

## 2.3 Accuracy

The accuracy of GLISTIN elevations was ground-truthed by differencing lidar DEMs from GLISTIN DEMs (Table SOM2). All lidar data were converted from its native coordinate system to WGS84 to UTM using Vdatum (Version 3.8, 2017, National Oceanic and Atmospheric Administration, Washington, DC), inducing an error of about 0.076 m (self-reported by Vdatum during conversion) and resampled to 3 m to match the GLISTIN DEMs spatial posting, using bilinear interpolation. To calculate elevation change the ⅓ arc-second NED was converted to UTM (WGS84) using Vdatum and resampled to 10 m using bilinear interpolation. GLISTIN and lidar elevations were also resampled to 10 m using bilinear interpolation to match the NED. The relative accuracy of GLISTIN, lidar, and the NED were inter-compared at four barren earth snow-free control zones in the Cascade Range of Oregon and Washington where all three estimates of elevation were available. Each control zone is a patchwork of co-located but isolated terrains. Barren earth terrains were derived from the ‘barren’ class of the 2016 National Land Cover Database (https://www.mrlc.gov/data/nlcd-2016-land-cover-conus). GLISTIN’s performance imaging ice/snow surfaces was examined by comparing elevations to lidar data acquired on Mount Adams, Washington, which was flown 28 days prior to the GLISTIN flights. We expect GLISTIN to yield somewhat lower elevations due to melting of the snow and ice.

## 2.4 Area and Volume Change

The reference area and elevation of the glaciers and perennial snowfields are derived from (Fountain et al., 2017) and a 'historic' version of the NED (Gesch et al., 2002), respectively. Both are based on the original U.S. Geological Survey 1:24000 topographic maps from which the glacier outlines and elevations were derived. The maps in the western US were drawn over a period of years (1940s-1980s. Resolution of the NED is ⅓ arc-second (~10 m), and the horizontal and vertical coordinate systems are North American Datum of 1983, North American Vertical Datum of 1988, respectively. The NED is continually being updated and it was necessary to retrieve the original 'historic' version from multiple sources (Table SOM1).

Volume change was estimated by differencing the GLISTIN elevations from the NED elevations within the original perimeter and for only those glaciers with ≥ 80% GLISTIN coverage. Le Bris and Paul (2015) showed that good estimates of volume change can be achieved with the elevation postings cover at least 80% of the glacier area. Reasonable estimates of volume change can be obtained for coverages as low as 40%, however results depend on interpolation method (McNabb et al., 2019), so we adopted the more conservative threshold of 80% used by Le Bris and Paul (2015). In order to compare volume loss between large and small glaciers and because the historic mapping occurred over a time-span of decades across the western US, results are expressed as the rate of specific volume (volume/area) change ($m^{-3}$ $m^{-2}$ $yr^{-1}$ or m $yr^{-1}$).

Uncertainty of volume change, $\sigma_{\Delta V}$, is calculated for each individual glacier or perennial snowfield, using the vertical and area uncertainties (Menounos et al., 2018),

$$\sigma_{\Delta V} = \sqrt{\left(\sigma_{\Delta z} A_g\right)^2 + (\sigma_A \Delta z)^2}\,, \qquad (1)$$

where $\sigma_{\Delta Z}$ is the RMSE of elevation differences between GLISTIN and the NED for all barren earth control zones, for the region in which the glacier or perennial snowfield is located, $A_g$ is the original (historic) area of the glacier or perennial snowfield, Δz is the average elevation change of the glacier or perennial snowfield, and $\sigma_A$ is area uncertainty. Uncertainty of the original areas is considered 9% (Fountain et al., 2017).

## 3. Results and Analysis

### 3.1 Data collection

The GLISTIN flights imaged the glacier-populated mountains of the American West for 5 flight days, between September 12 to 28, 2016, covering about 41,000 $km^2$ (Figure 1). Due to an unexpected reassignment of the aircraft, several mountain ranges were not included, most notably the Olympic Mountains, WA, and the Absaroka Range, WY. Within the regions surveyed 3889 glaciers and perennial snowfields are present. GLISTIN coverage of each varied from 0 to 100% with a median of 81%. The total number of features with ≥ 80% coverage was 1770 (309 $km^2$, 53% of the total area of surveyed G&PS; figure 2).

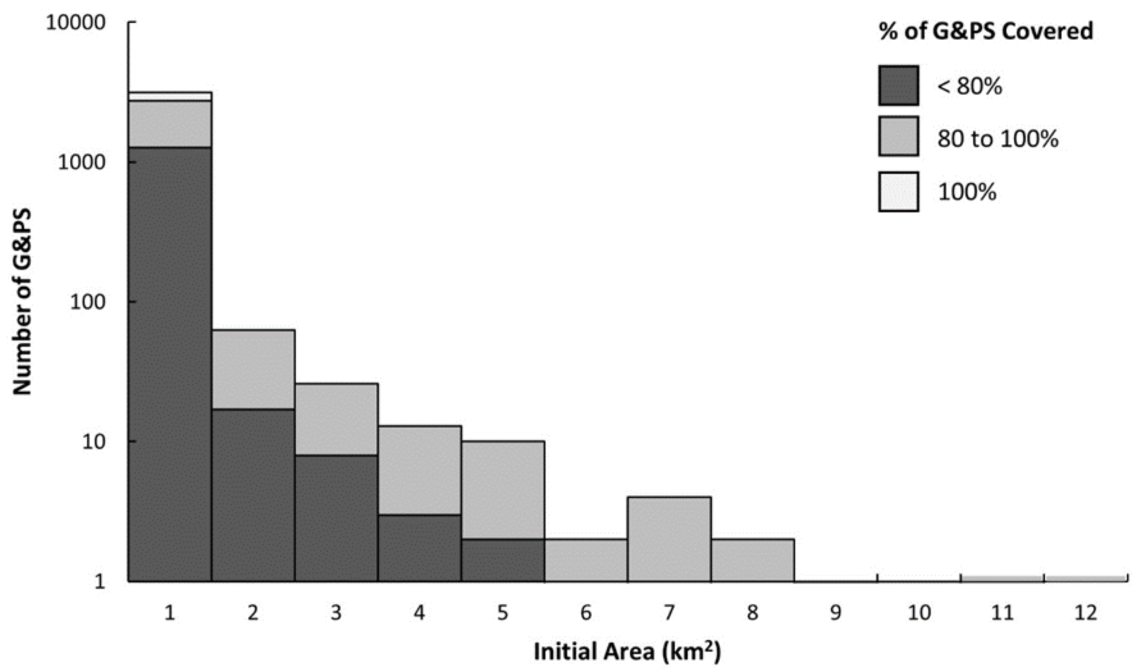


**Figure 2.** Histogram of the initial area of glaciers and perennial snowfields and the fraction of area mapped by GLISTIN. Initial area refers to the area from the U.S. Geological Survey's 1:24000 map series. The x-axis value is the maximum for each bin.

As expected, increasing the number of flight passes over the same area increased the backscatter coverage. For one flight pass backscatter was received from 17% of the entire illuminated area, for two flights 66%, four flights, 86%, and for eight flights 94% (Table SOM3). No significant difference was observed in backscatter coverage of snow/ice surfaces compared to ice-free surfaces, and within glaciers no significant differences between snow-covered regions and ice-exposed regions. Backscatter reception was only significantly correlated with terrain slope with greater loss on steeper slopes.

## 3.2 Accuracy

The GLISTIN DEMs for three of the four barren earth control zones were compiled from multiple passes. The fourth control zone (Mount Adams, WA) was comprised of single pass data and was examined separately. For the three multi-pass barren earth control zones the GLISTIN – lidar (3 m posting) mean difference was +0.17 ± 1.78 m (Table SOM4). Comparing GLISTIN and the NED over the same regions (10 m posting), the mean difference and standard deviation was much larger, +1.05 ± 6.38 m. This is due to the much larger uncertainty in the NED elevations of 3.74 m, which is based mostly on control points located in lower elevation and less complex terrain (Gesch, 2007). The mean lidar-NED difference -0.89 ± 5.83, supports this inference. For the control zones on Mount Adams, the mean elevations difference of single-pass GLISTIN - lidar (3 m posting) was -0.00 ± 3.20 m, whereas for the snow/ice surfaces it was -0.86 ± 3.76 m. The negative difference for the snow/ice surfaces is to be expected given the melting that occurred over the 28-day period between the initial lidar survey followed by the GLISTIN survey. Given that the snow is wet during this time of year and interferometric penetration is negligible (Hensley et al., 2016).

With respect to interferometric radar errors it is important to note that the height precision is dominated by the instrument random noise. This relative error is high frequency and will scale with spatial averaging of uncorrelated pixels or independent samples.  The same is not true for the height accuracy or systematic (mean) offset which does not improve with averaging as they are correlated. Therefore, if we calculate the RMSE for more coarse spatial postings this metric will reduce significantly (with the random /precision inversely proportional to the square-root of the effective number of independent looks (Hensley et. al. 2016). For this paper we analyze GLISTIN data at a spatial posting of 3m due to the small footprint of many of these glaciers. However, one can expect significantly improved height precision, and thereby RMSE for large glaciers via spatial averaging. The low mean difference (i.e. accuracy) observed for the barren areas indicates that extremely low height errors are achievable with sufficient spatial averaging to reduce the random component (Schumann et. al. 2016; Moller et.al. 2019)

Although no correlation was observed between mean elevation difference (GLISTIN - lidar) and surface slope, the standard deviation increased from about 1.7 m for slopes between 20° and $30^{o}$ to 3.8 m for slopes between 50° and $60^{o}$. The RMSE (GLISTIN-NED) increased from 6.1 m for slopes 20° to $30^{o}$ to 10.2 m for slopes between 50° and $60^{o}$. The rate of phase change is a function of the interferometric measurement geometry and is directly proportional to the local slope. Phase unwrapping becomes more difficult as the slope increases so an increased RMSE in extreme topography is to be expected. The orientation of single-pass GLISTIN relative to the terrain surface affects the elevation difference. The mean elevation difference (GLISTIN-lidar) was smaller for surfaces facing towards GLISTIN, +0.01 ± 2.07 m, than surfaces facing away, +0.07 ± 4.03 m.

### 3.3 Volume change

Volume change was estimated for 1770 glaciers and perennial snowfields (54% of total) consisting of 351 glaciers and 1419 snowfields. Overall mean uncertainty, based on barren earth control zones across the west (Table SOM5), was -0.37 ± 7.31 m. Rejecting those specific volume changes that were smaller than uncertainty yielded 231 glaciers totaling 198.84 $km^2$ and 551 perennial snowfields (21.31 $km^2$). Comparing our volume change to a prior estimate for Mt. Rainier, Washington (Sisson et al., 2011), showed that the prior estimate, based on a lidar-NED difference, of -8.6 m (1970-2007) is within the uncertainty of our value , -9.7 ± 4.8 m (1970-2016). That our estimate showed a greater mass loss is consistent with the longer time period of comparison.

Most glaciers and perennial snowfields lost mass (Figure 3). The median rate of change for glaciers, -0.3 ± 0.2 m $yr^{-1}$, and for snowfields, -0.2 ± 0.2 m $yr^{-1}$. Four glaciers (2%) and 56 (10%) perennial snowfields increased in volume; their locations are not region specific. These features are characterized by small area, median 0.02 $km^2$ (all but one < 0.2 $km^2$), steeper slopes, and higher elevations. The features that gained volume were at significantly higher elevations and steeper slopes (median 3100 m, 28°) compared to those that lost volume, (median 2335 m 25°; $p < 0.05$, Mann-Whitney U). The time series of ice mass loss in the Cascade Range, Washington is relatively complete compared to other regions and show increasing mass loss with time (Figure 4). The rate of change increased significantly since 1980.

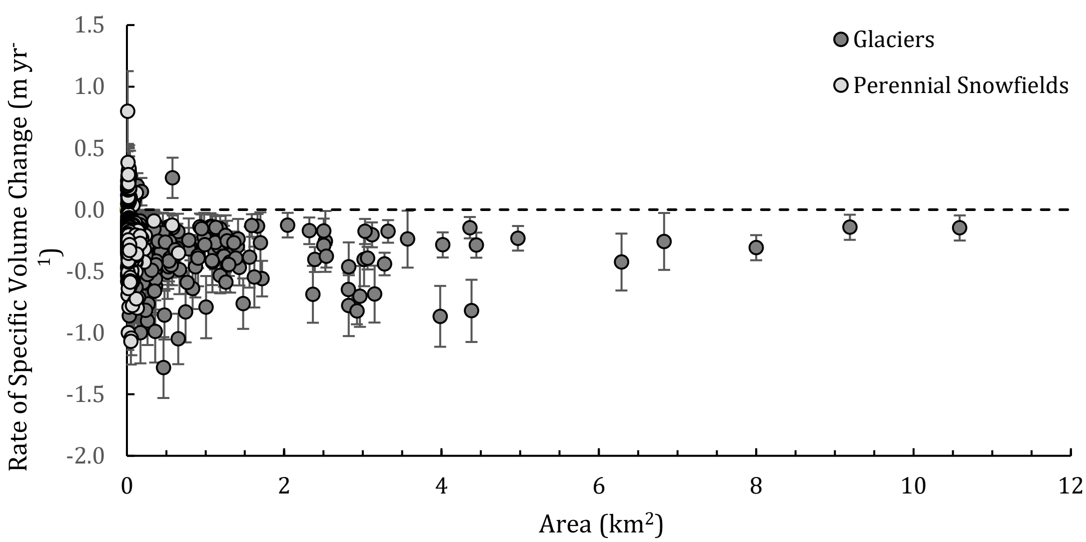


**Figure 3.** Specific volume change of glaciers and perennial snowfields (G&PS). Light grey circles represent perennial snowfields, and dark grey circles represent glaciers. The 'whiskers' represent uncertainty. Initial area refers to the area from the U.S. Geological Survey's 1:24000 map series.

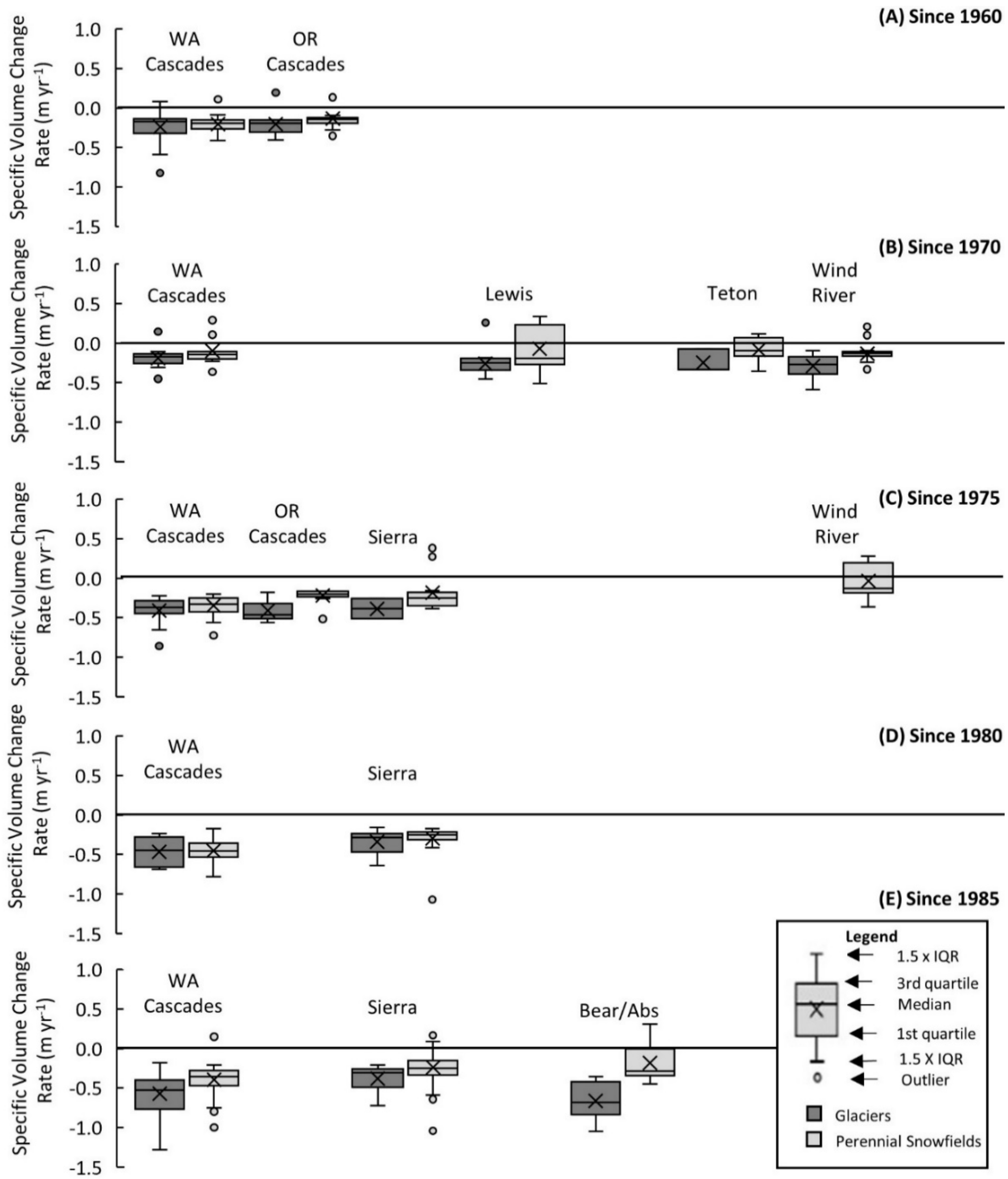


**Figure 4.** Volume change glaciers (dark grey boxes) and perennial snowfields (light grey boxes for each region with more than ten features, grouped by initial mapping date (all ending in 2016), 1960 (1956 to 1960) (A), 1970 (1966 to 1970) (B), 1975 (1971 to 1975) (C), 1980 (1976 to 1980) (D), and 1985 (1981 to 1985) (E). The 'whiskers' represent the smallest and largest values not considered outliers. The values that exceed 1.5 times the interquartile range (IQR) below the first quartile or above the third quartile are considered outliers (open circles 'Bear/Abs' refers to Beartooth-Absaroka, MT.

## 4. Discussion and Conclusions

GLISTIN was developed for measuring the relatively flat surfaces of large glaciers and ice sheets, and its application to the complex topography alpine terrain presents a stress-case for the instrument. GLISTIN elevation mosaics compared favorably to lidar measurements over barren earth +0.17 ± 1.78 m (3 m posting). Similar comparisons over bedrock in Greenland showed, +0.32 ± 0.95 m (30 m posting) for single pass elevations (Moller et al., 2019). Over snow and ice surfaces on Mount Adams the mean difference of GLISTIN and lidar was -0.87 ± 3.8 m (3 m posting). We regard much of the difference due to snow and ice melt over the 28-day interval between the initial lidar and later GLISTIN surveys. Similar mean GLISTIN – lidar differences, were observed on two gently sloping glacier surfaces in Alaska, +0.8 ± 1.7 m and +1.2 ± 3.7 m (3 m posting, Moller et al., 2019). There was a similarly substantial time interval between the GLISTIN and subsequent lidar surveys of 1.5 month and 1 month, respectively. Differencing GLISTIN from the NED for estimating historic glacier change showed the RMSE at control zones to be 7.35 m and largely driven by uncertainty in the NED.

The standard deviations for all elevation comparisons increased with surface slope and most likely due to small offsets in aligning the DEMs. This result is also common to other studies using matching DEMs. The mean elevation difference (Shuttle Radar Topography Mission 1 Arc-Second Global DEM) over non-glaciated terrain near the Akshiirak glaciers (Tien Shan, Central Asia) was -4.5 ± 10.9 m for slopes between 25° and 30°, increasing to -7.6 ± 25.6 m for slopes between 40°and 78° (Paul, 2008; Surazakov & Aizen, 2006). For North & Middle Sisters, Oregon the RMSE (lidar-NED) was 5.7 m and 12.3 m for slopes between 20° to 30° and 50° to 60°, respectively (Ohlschlager, 2015), and similar to the GLISTIN-NED RMSE of 6.4 m and 10.2 m for the same slope bins.

Elevations were acquired for 85% of the surveyed glaciers and perennial snowfields, of which 12% were completely mapped and 60% had ≥ 80% coverage. Increased number of flight passes increased data coverage. This is one clear advantage over satellite InSAR that look direction can be easily changed. Most of the missing backscatter was caused by radar shadow and some from layover due to the steep terrain.

Rates of glacier specific mass loss across the western US are consistent with rates estimated by other studies in our region. Overall, our rates over the last period of our study 1985 - 2016 are consistent with the western US average (2000-2020) of about -0.4 m $yr^{-1}$ (Hugonnet et al., 2021). For the Cascade Range in Washington, Menounos et al. (2018) estimated -0. 29 ± 0.10 m $yr^{-1}$ (2000-2018) from DEMs derived from optical satellite imagery, which is half of our estimate of -0.63 ± 0.26 m $yr^{-1}$ over the longer time period of 1985-2016. Furthermore, our historic (pre-2000) rates of change is similar to rates elsewhere globally (Andreassen et al., 2020; Carturan et al., 2013; DeBEER & Sharp, 2007; Lambrecht & Kuhn, 2007). We also note an acceleration in mass loss since 1980.

GLISTIN makes an important contribution in tracking glacier change because data can be rapidly collected unimpeded by weather providing a near instantaneous elevation survey of glaciers across broad regions. It performed well in complex terrain exceeding its design requirement and future improvements in flight planning will reduce the uncertainty. Significantly improved uncertainty for larger glaciers is expected due to spatial averaging that reduces the random error component.

**Acknowledgments**

This work was supported by NASA grant NNX17AI59G. The authors would like to thank Yang Zhen and the GLISTIN group at JPL for their help in data processing and interpretation.

**Data Availability Statement**

Analyzed data are included as Supporting Information S1. The single radar swaths of elevation can be obtained from NASA, https://uavsar.jpl.nasa.gov/cgi-bin/data.pl, select

TopSAR (Ka-band). The mosaicked radar swaths used in this study can be found at, https://pdxscholar.library.pdx.edu/geology_data/5/. The reference glacier outlines and elevations derived from the historic 1:24,000 USGS topographic maps and historic National Elevation Dataset (NED), respectively are located at, https://pdxscholar.library.pdx.edu/geology_data/4/ .

## References


Andreassen, L. M., Elvehøy, H., Kjøllmoen, B., & Belart, J. M. C. (2020). Glacier change in Norway since the 1960s – an overview of mass balance, area, length and surface elevation changes. *Journal of Glaciology*, *66*(256), 313–328. https://doi.org/10.1017/jog.2020.10

Andreassen, L. M., Elvehøy, H., Kjøllmoen, B., Engeset, R. V., & Haakensen, N. (2005). Glacier mass-balance and length variation in Norway. *Annals of Glaciology*, *42*, 317–325. https://doi.org/10.3189/172756405781812826

Basagic, H. J., & Fountain, A. G. (2011). Quantifying 20th Century Glacier Change in the Sierra Nevada, California. *Arctic, Antarctic, and Alpine Research*, *43*(3), 317–330. https://doi.org/10.1657/1938-4246-43.3.317

Carturan, L., Filippi, R., Seppi, R., Gabrielli, P., Notarnicola, C., Bertoldi, L., Paul, F., Rastner, P., Cazorzi, F., Dinale, R., & Dalla Fontana, G. (2013). Area and volume loss of the glaciers in the Ortles-Cevedale group (Eastern Italian Alps): Controls and imbalance of the remaining glaciers. *The Cryosphere*, *7*(5), 1339–1359. https://doi.org/10.5194/tc-7-1339-2013

DeBEER, C. M., & Sharp, M. J. (2007). Recent changes in glacier area and volume within the southern Canadian Cordillera. *Annals of Glaciology*, *46*(1), 215–221. https://doi.org/10.3189/172756407782871710

DeVisser, M. H., & Fountain, A. G. (2015). A century of glacier change in the Wind River Range, WY. *Geomorphology*, *232*, 103–116. https://doi.org/10.1016/j.geomorph.2014.10.017

Eineder, M., & Holzner, J. (2000). Interferometric DEMs in alpine terrain-limits and options for ERS and SRTM. *IGARSS 2000. IEEE 2000 International Geoscience and Remote Sensing Symposium. Taking the Pulse of the Planet: The Role of Remote Sensing in Managing the Environment. Proceedings (Cat. No.00CH37120)*, *7*, 3210–3212 vol.7. https://doi.org/10.1109/IGARSS.2000.860385

Fagre, D. B., McKeon, L. A., Dick, K. A., & Fountain, A. G. (2017). *Glacier margin time series (1966, 1998, 2005, 2015) of the named glaciers of Glacier National Park, MT, USA* [Data set]. U.S. Geological Survey. https://doi.org/10.5066/f7p26wb1

Fountain, A. G., Glenn, B., & Basagic, H. J. (2017). The Geography of Glaciers and Perennial Snowfields in the American West. *Arctic, Antarctic, and Alpine Research*, *49*(3), 391–410. https://doi.org/10.1657/AAAR0017-003

Fountain, A. G., & Tangborn, W. V. (1985). The effect of glaciers on streamflow variations. *Water Resources Research*, *21*(4), 579–586.

Gesch, D., Oimoen, M., Greenlee, S., Nelson, C., Steuck, M., & Tyler, D. (2002). The national elevation dataset. *Photogrammetric Engineering and Remote Sensing*, *68*(1), 5–32.

Hall, M. H., & Fagre, D. B. (2003). Modeled climate-induced glacier change in Glacier National Park, 1850–2100. *BioScience*, *53*(2), 131–140.

Hensley, S., Moller, D., Oveisgharan, S., Michel, T., & Wu, X. (2016). Ka-Band Mapping and Measurements of Interferometric Penetration of the Greenland Ice Sheets by the GLISTIN Radar. *IEEE Journal of Selected Topics in Applied Earth Observations and Remote Sensing*, *9*(6), 2436–2450. https://doi.org/10.1109/JSTARS.2016.2560626

Hoffman, M. J., Fountain, A. G., & Achuff, J. M. (2007). 20th-century variations in area of cirque glaciers and glacierets, Rocky Mountain National Park, Rocky Mountains, Colorado, USA. *Annals of Glaciology*, *46*(1), 349–354. https://doi.org/10.3189/172756407782871233

Hugonnet, R., McNabb, R., Berthier, E., Menounos, B., Nuth, C., Girod, L., Farinotti, D., Huss, M., Dussaillant, I., Brun, F., & Kääb, A. (2021). Accelerated global glacier mass loss in the early twenty-first century. *Nature*, *592*(7856), 726–731. https://doi.org/10.1038/s41586-021-03436-z

Kaser, G., Fountain, A. G., & Jansson, P. (2003). *A manual for monitoring the mass balance of mountain glaciers* (No. 59; IHP-VI Technical Documents in Hydrology, p. 137). UNESCO.

Lambrecht, A., & Kuhn, M. (2007). Glacier changes in the Austrian Alps during the last three decades, derived from the new Austrian glacier inventory. *Annals of Glaciology*, *46*(1), 177–184.

Le Bris, R., & Paul, F. (2015). Glacier-specific elevation changes in parts of western Alaska. *Annals of Glaciology*, *56*(70), 184–192. https://doi.org/10.3189/2015AoG70A227

McNabb, R., Nuth, C., Kääb, A., & Girod, L. (2019). Sensitivity of glacier volume change estimation to DEM void interpolation. *The Cryosphere*, *13*(3), 895–910. https://doi.org/10.5194/tc-13-895-2019

Meier, M. F. (1984). Contribution of small glaciers to global sea level. *Science*, *226*(4681), 1418–1421.

Menounos, B., Hugonnet, R., Shean, D., Gardner, A., Howat, I., Berthier, E., Pelto, B., Tennant, C., Shea, J., Noh, M., Brun, F., & Dehecq, A. (2018). Heterogeneous changes in western North American glaciers linked to decadal variability in zonal wind strength. *Geophysical Research Letters*. https://doi.org/10.1029/2018GL080942

Millan, R., Mouginot, J., Rabatel, A., & Morlighem, M. (2022). Ice velocity and thickness of the world's glaciers. *Nature Geoscience*, *15*(2), 124–129. https://doi.org/10.1038/s41561-021-00885-z

Moller, D., Andreadis, K. M., Bormann, K. J., Hensley, S., & Painter, T. H. (2017). Mapping Snow Depth From Ka-Band Interferometry: Proof of Concept and Comparison With Scanning Lidar Retrievals. *IEEE Geoscience and Remote Sensing Letters*, *14*(6), 886–890.

Moller, D., Hensley, S., Mouginot, J., Willis, J., Wu, X., Larsen, C., Rignot, E., Muellerschoen, R., & Khazendar, A. (2019). Validation of Glacier Topographic

Acquisitions from an Airborne Single-Pass Interferometer. *Sensors*, *19*(17), 3700. https://doi.org/10.3390/s19173700

Moller, D., Hensley, S., Sadowy, G., Fisher, C., Michel, T., Zawadzki, M., & Rignot, E. (2011). The Glacier and Land Ice Surface Topography Interferometer: An Airborne Proof-of-Concept Demonstration of High-Precision Ka-Band Single-Pass Elevation Mapping. *Geoscience and Remote Sensing, IEEE Transactions On*, *49*, 827–842. https://doi.org/10.1109/TGRS.2010.2057254

Moore, R. D., Fleming, S. W., Menounos, B., Wheate, R., Fountain, A., Stahl, K., Holm, K., & Jakob, M. (2009). Glacier change in western North America: Influences on hydrology, geomorphic hazards and water quality. *Hydrological Processes*, *23*(1), 42–61. https://doi.org/10.1002/hyp.7162

Mouginot, J., Rignot, E., Bjørk, A. A., van den Broeke, M., Millan, R., Morlighem, M., Noël, B., Scheuchl, B., & Wood, M. (2019). Forty-six years of Greenland Ice Sheet mass balance from 1972 to 2018. *Proceedings of the National Academy of Sciences*, *116*(19), 9239–9244. https://doi.org/10.1073/pnas.1904242116

Ohlschlager, J. G. (2015). *Glacier Change on the Three Sisters Volcanoes, Oregon: 1900–2010* [ProQuest Dissertations Publishing]. https://search.proquest.com/docview/1718552424?pq-origsite=primo

O'Neal, M. A., Hanson, B., Carisio, S., & Satinsky, A. (2015). Detecting recent changes in the areal extent of North Cascades glaciers, USA. *Quaternary Research*, *84*(2), 151–158. https://doi.org/10.1016/j.yqres.2015.05.007

O'Neel, S., McNeil, C., Sass, L. C., Florentine, C., Baker, E. H., Peitzsch, E., McGrath, D., Fountain, A. G., & Fagre, D. (2019). Reanalysis of the US Geological Survey Benchmark Glaciers: Long-term insight into climate forcing of glacier mass balance. *Journal of Glaciology*, *65*(253), 850–866. https://doi.org/10.1017/jog.2019.66

Ostrem, G., & Brugman, M. (1991). *Glacier mass balance measurements: A manual for field and office work* (Science Report No. 4; p. 224). National Hydrology Research Institute,.

Paul, F. (2008). Calculation of glacier elevation changes with SRTM: Is there an elevation-dependent bias? *Journal of Glaciology*, *54*(188), 945–946.

Pfeffer, W. T., Arendt, A. A., Bliss, A., Bolch, T., Cogley, J. G., Gardner, A. S., Hagen, J.-O., Hock, R., Kaser, G., & Kienholz, C. (2014). The Randolph Glacier Inventory: A globally complete inventory of glaciers. *Journal of Glaciology*, *60*(221), 537–552. https://doi.org/10.3189/2014JoG13J176

Rees, W. G. (2000). Technical note: Simple masks for shadowing and highlighting in SAR images. *International Journal of Remote Sensing*, *21*(11), 2145–2152. https://doi.org/10.1080/01431160050029477

Rosen, P. A., Hensley, S., Joughin, I. R., Li, F. K., Madsen, S. N., Rodriguez, E., & Goldstein, R. M. (2000). Synthetic aperture radar interferometry. *Proceedings of the IEEE*, *88*(3), 333–382. https://doi.org/10.1109/5.838084

Schumann, G. J.-P., Moller, D. K., & Mentgen, F. (2016). High-Accuracy Elevation Data at Large Scales from Airborne Single-Pass SAR Interferometry. *Frontiers in Earth Science*, *3*. https://doi.org/10.3389/feart.2015.00088

Shepherd, A., Ivins, E., Rignot, E., Smith, B., Van Den Broeke, M., Velicogna, I., Whitehouse, P., Briggs, K., Joughin, I., & Krinner, G. (2018). Mass balance of the Antarctic Ice Sheet from 1992 to 2017. *Nature*, *558*, 219–222.

Sisson, T. W., Robinson, J. E., & Swinney, D. D. (2011). Whole-edifice ice volume change AD 1970 to 2007/2008 at Mount Rainier, Washington, based on LiDAR surveying. *Geology*, *39*(7), 639–642.

Surazakov, A. B., & Aizen, V. B. (2006). Estimating volume change of mountain glaciers using SRTM and map-based topographic data. *IEEE Transactions on Geoscience and Remote Sensing*, *44*(10), 2991–2995.

Zemp, M., Huss, M., Thibert, E., Eckert, N., McNabb, R., Huber, J., Barandun, M., Machguth, H., Nussbaumer, S. U., Gärtner-Roer, I., Thomson, L., Paul, F., Maussion, F., Kutuzov, S., & Cogley, J. G. (2019). Global glacier mass changes and their contributions to sea-level rise from 1961 to 2016. *Nature*, *568*(7752), 382–386. https://doi.org/10.1038/s41586-019-1071-0

**Supplementary Online Material**

To identify the date of each glacier DEM, the glacier outlines were combined with a shapefile of the NED metadata (https://viewer.nationalmap.gov/basic) in ArcGIS (ESRI, Inc.). The NED from non-USGS sources (Table SOM1) did not include metadata for the imagery date. In those cases, we used the dates listed on the map collars of the USGS 1:24000 topographic maps. Often the same aerial photographs used to create the topographic maps were also used to derive the NED. Photography used to create the portion of the NED overlapping the GLISTIN surveys were flown between 1950-1993, with only two glaciers surveyed in 1950 (Wind River Range, WY) and nine after 1990 (Sierra Nevada, CA). There were 108 glacier outlines where the NED was derived from imagery spanning multiple years, of which 23 had USGS metadata, clearly identifying which portion of the outline corresponds with which year. The DEMs covering the remaining 85 glaciers were from non-USGS sources, and it is unclear what portion of the glacier were covered by imagery from which year. For G&PS, where multiple images were used to create the NED, if >80% of the G&PS area was imaged within a single year (21 G&PS), that year defined the date. For the remaining 64 G&PS, the date is defined as the average of all years listed. The reported RMSE of the NED (1999 version) is 3.74 m, but that RMSE under samples high elevation and slopes, fewer than ten samples for slope > 30°, and ~20 samples for elevations > 3000 m (Gesch, 2007). Therefore, the error over glaciers and the surrounding alpine environment is probably much higher.

The NED was split into regions corresponding to the mountain ranges covered by GLISTIN. In some cases, regions were split into smaller sub-regions to reduce processing time. Each was converted to the same vertical reference system as GLISTIN (WGS84) using Vdatum then projected into the UTM coordinate system and resampled to 10 m using bilinear interpolation. The pixel resolution was resampled to 10 m so that it was standard across all regions. Before resampling, the pixel resolution of the NED differed by region, ranging from 8.5 m (northern Cascades, WA) to 9.4 m (Sierra Nevada, CA). GLISTIN was also resampled to 10 m and co-registered to the NED using the methods of

Berthier et al. (2007). The co-registration process reduces the horizontal and vertical offsets between the DEMs by first minimizing the standard deviation of differences over control zones and then applying that shift to the whole DEM. Offsets between DEMs can significantly influence estimates of elevation change, particularly on steep slopes (Berthier et al., 2007).

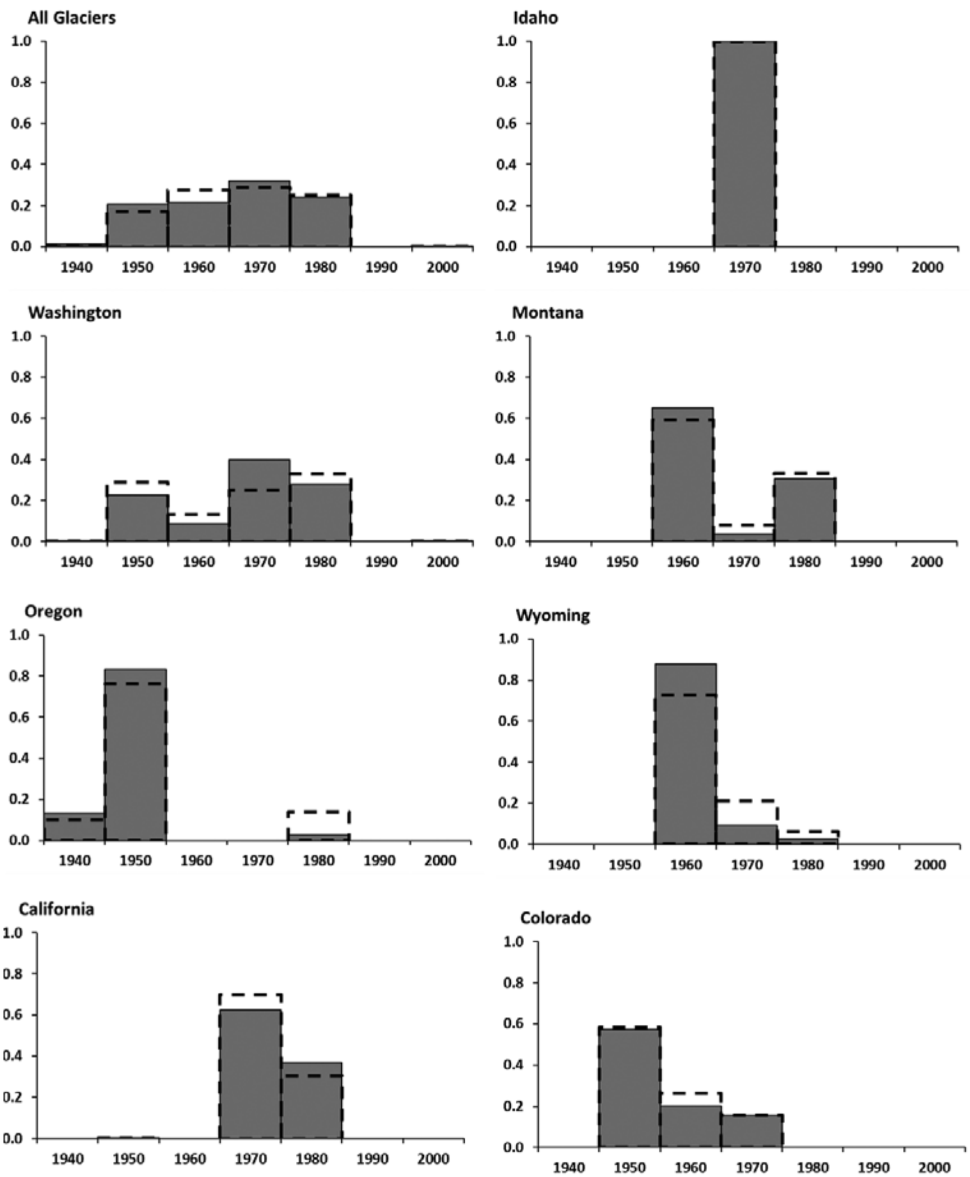


**Figure SOM1.** Acquisition dates for imagery used to create the U.S. Geological Survey 1:24000 topographic maps for areas with glaciers and perennial snowfields (G&PS). The date on the x-axis represents the full decade (e.g., 1960 = 1960 to 1969). The y-axis is the fraction of the total. The solid grey bars are the fraction of area, and the dashed outline is the fraction of the number of G&PS. The top left depicts the imagery for all G&PS in the western U.S. The other graphs show the acquisition date for each state. Reprinted from Fountain et al. (2017).

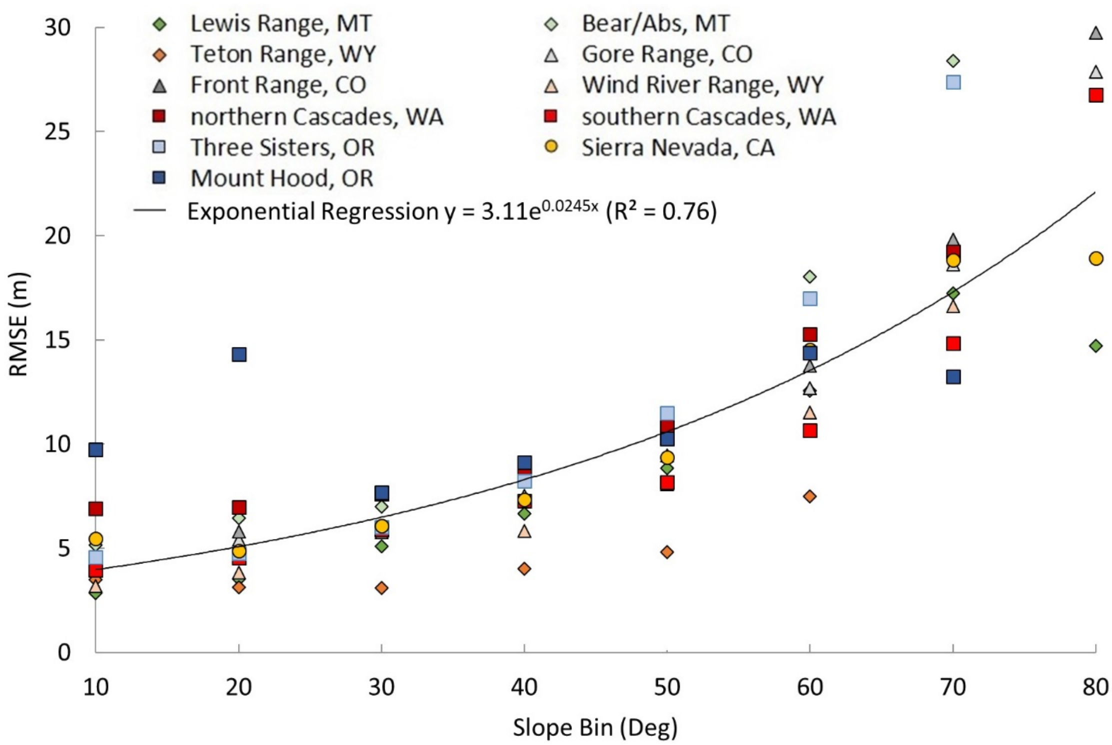


**Figure SOM2.** Root mean square error (RMSE) between GLISTIN elevations and the National Elevation Dataset for control zones binned by 10° slopes. The slope label represents the maximum of that bin. The 10° slope bin includes slopes of 0°.

**Table SOM1.** List of sources compiled for the historical elevation data. The three sources used were the National Map, maintained by the U.S. Geological Survey (USGS), the Oregon office of the Bureau of Land Management (BLM), and the Geomorphological Research Group at the University of Washington (UW).

| State/Range | Source | Website |
|---|---|---|
| **California** | | |
| Sierra Nevada | USGS | https://viewer.nationalmap.gov/basic |
| **Colorado** | | |
| Front | USGS | https://viewer.nationalmap.gov/basic |
| Gore | USGS | https://viewer.nationalmap.gov/basic |
| **Montana** | | |
| Beartooth-Absaroka | USGS | https://viewer.nationalmap.gov/basic |
| Lewis | USGS | https://viewer.nationalmap.gov/basic |
| **Oregon** | | |
| Cascade | BLM | http://earthexplorer.usgs.gov |
| **Washington** | | |
| northern Cascades | UW | http://gis.ess.washington.edu/data/ |
| northern Cascades | USGS | https://viewer.nationalmap.gov/basic |
| southern Cascades | BLM | http://earthexplorer.usgs.gov |
| **Wyoming** | | |
| Teton | USGS | https://viewer.nationalmap.gov/basic |
| Wind River | USGS | https://viewer.nationalmap.gov/basic |

**Table SOM2**. List of lidar datasets used for the absolute error assessment. The datasets came from three sources, the National Map, maintained by the U.S. Geological Survey (USGS; https://viewer.nationalmap.gov/basic/), Washington Department of Natural Resources (WA DNR; https://lidarportal.dnr.wa.gov/), and Oregon Department of Geology and Mineral Industries (DOGAMI; https://gis.dogami.oregon.gov/maps/lidarviewer/). 'Uncertainty' refers to the reported absolute vertical uncertainty of the lidar.

| Region | Year | Source | Uncertainty |
|---|---|---|---|
| Mount Adams, WA | 2016 | USGS | 0.07 |
| northern Cascade Range, WA | 2009 | WA DNR | 0.04 |
| Mount Rainier, WA | 2007/2008 | WA DNR | 0.04 |
| Three Sisters, OR | 2010 | DOGAMI | 0.04 |

**Table SOM3.** Amount of missing data in GLISTIN mosaic based on the number of flight passes. 'Missing Area' is the total area of pixels for the listed category in the GLISTIN mosaic that had no elevation data. 'Total Area' is the total area of all pixels for the category in the GLISTIN mosaic. '% Missing' is the ratio of the missing area divided by the total area within that category.

| **Flight Passes** | **Missing Area ($km^2$)** | **Total Area ($km^2$)** | **% Missing** |
|---|---|---|---|
| 1 | 8575.94 | 10259.58 | 83.59 |
| 2 | 5368.17 | 15877.95 | 33.81 |
| 3 | 1167.58 | 7344.92 | 15.90 |
| 4 | 912.02 | 6511.64 | 14.01 |
| 5 | 154.29 | 813.70 | 18.96 |
| 6 | 51.56 | 379.55 | 13.59 |
| 7 | 8.67 | 147.40 | 5.88 |
| 8 | 4.00 | 64.31 | 6.23 |

**Table SOM4.** Elevation uncertainty for control zones estimated from comparing GLISTIN, lidar, and National Elevation Dataset (NED). The sources and accuracy of the lidar data are listed in the supplementary online material. 'Region' refers to the region of the mosaicked GLISTIN digital elevation models, 'Area' is the area of the control zone, 'Swath Count' is a range of the number of GLISTIN flights covering the control zones, and standard deviation, 'RMSE' is the root mean square error. The 'All' column combines data from the three regions (columns to the left) with multiple GLISTIN passes.

| | northern Cascades, WA | Mount Rainier, WA | Three Sisters, OR | All | Mount Adams, WA |
|---|---|---|---|---|---|
| Lidar Year | 2009 | 2007/08 | 2010 | --- | 2016 |
| Area ($km^2$) | 1.61 | 3.10 | 1.95 | 6.66 | 12.74 |
| Swath Count | 3-6 | 3-4 | 2 | 2-6 | 1 |
| **GLISTIN minus lidar** | | | | | |
| RMSE (m) | +1.79 | +1.87 | +1.64 | +1.78 | +3.20 |
| Mean ± std (m) | -0.14 ± 1.78 | +0.38 ± 1.83 | +0.10 ± 1.63 | +0.17 ± 1.78 | 0.00 ± 3.20 |
| Median (m) | -0.08 | +0.17 | +0.15 | +0.11 | 0.00 |
| **GLISTIN minus NED** | | | | | |
| RMSE (m) | +8.84 | +3.36 | +7.14 | +6.46 | +6.22 |
| Mean ± std (m) | +4.49 ± 7.61 | +0.57 ± 3.31 | -2.05 ± 6.84 | +1.05 ± 6.38 | +0.49 ± 6.20 |
| Median (m) | +4.83 | +035 | -0.49 | +0.80 | +0.52 |
| **Lidar minus NED** | | | | | |
| RMSE (m) | +7.21 | +2.27 | +8.37 | +5.89 | +5.60 |
| Mean ± std (m) | +0.13 ± 7.21 | -0.21 ± 2.27 | -2.87 ± 7.86 | -0.89 ± 5.83 | -0.18 ± 5.60 |
| Median (m) | +0.54 | -0.15 | -0.62 | -0.19 | -0.03 |

**Table SOM5.** Root mean square error (RMSE), and mean elevation difference between the National Elevation Dataset and GLISTIN derived elevations of barren earth control zones, and total area (Area) of the barren earth control zones in each region sampled.

| **Region** | **RMSE (m)** | **Mean ± std (m)** | **Area ($km^2$)** |
|---|---|---|---|
| northern Cascades, WA | 7.74 | +0.33 ± 7.73 | 107.34 |
| southern Cascades, WA | 5.81 | +0.62 ± 5.83 | 27.06 |
| Mount Hood, OR | 8.26 | -2.42 ± 8.25 | 10.21 |
| Three Sisters, OR | 6.07 | +0.64 ± 6.03 | 23.19 |
| Sierra Nevada, CA | 6.64 | -1.72 ± 6.42 | 191.16 |
| Lewis, MT | 8.89 | +1.72 ± 8.80 | 22.16 |
| Beartooth-Absaroka, MT | 10.57 | -0.26 ± 10.57 | 7.83 |
| Teton, WY | 3.53 | -0.32 ± 3.52 | 0.93 |
| Wind River, WY | 6.55 | -0.96 ± 6.48 | 7.81 |
| Front, CO | 8.31 | +1.40 ± 8.19 | 36.54 |
| Gore, CO | 8.15 | +1.68 ± 7.98 | 27.43 |
| Total | **7.32** | **-0.37 ± 7.31** | **461.67** |

**Table SOM6.** Volume change estimates for glaciers and perennial snowfields in select regions and periods. Volume change was estimated between the initial NED year and the GLISTIN year of 2016 for glaciers and perennial snowfields with ≥ 80% GLISTIN. The change was grouped by region and year. The year listed is the last in the 5-year interval (e.g., 1955 = 1951 to 1955). 'Num' is the number of G&PS for that category.

| Region/Year/Type | Num | Area ($km^2$) | Volume Change ($m^3$ x $10^6$) | Specific Vol Change (m) | Specific Vol Change Rate (m $yr^{-1}$) |
|---|---|---|---|---|---|
| **WA Cascades** | | | | | |
| 1960 | 75 | 19.70 | -336.81 ± 117.49 | -17.10 ± 5.96 | -0.31 ± 0.11 |
| Glacier | 29 | 17.75 | -312.42 ± 106.56 | -17.60 ± 6.00 | -0.31 ± 0.11 |
| Snowfield | 46 | 1.95 | -24.40 ± 10.93 | -12.48 ± 5.59 | -0.22 ± 0.10 |
| 1970 | 53 | 53.36 | -507.94 ± 255.44 | -9.52 ± 4.79 | -0.21 ± 0.10 |
| Glacier | 23 | 52.40 | -501.59 ± 250.65 | -9.57 ± 4.78 | -0.21 ± 0.10 |
| Snowfield | 30 | 0.96 | -6.35 ± 4.79 | -6.62 ± 5.00 | -0.14 ± 0.11 |
| 1975 | 82 | 15.88 | -290.34 ± 124.61 | -18.29 ± 7.85 | -0.45 ± 0.19 |
| Glacier | 24 | 13.14 | -249.19 ± 102.35 | -18.96 ± 7.79 | -0.46 ± 0.19 |
| Snowfield | 58 | 2.73 | -41.16 ± 22.26 | -15.05 ± 8.14 | -0.37 ± 0.20 |
| 1980 | 20 | 21.40 | -320.08 ± 180.75 | -14.95 ± 8.44 | -0.42 ± 0.23 |
| Glacier | 8 | 20.81 | -309.81 ± 175.82 | -14.89 ± 8.45 | -0.41 ± 0.23 |
| Snowfield | 12 | 0.59 | -10.27 ± 4.94 | -17.32 ± 8.33 | -0.48 ± 0.23 |
| 1985 | 101 | 34.14 | -662.12 ± 275.94 | -19.39 ± 8.08 | -0.63 ± 0.26 |
| Glacier | 40 | 31.54 | -628.40 ± 257.10 | -19.92 ± 8.15 | -0.64 ± 0.26 |
| Snowfield | 61 | 2.60 | -33.71 ± 18.83 | -12.97 ± 7.25 | -0.42 ± 0.23 |
| **OR Cascades** | | | | | |
| 1960 | 44 | 14.47 | -215.07 ± 90.29 | -14.86 ± 6.24 | -0.27 ± 0.11 |
| Glacier | 13 | 12.19 | -188.44 ± 76.15 | -15.46 ± 6.25 | -0.28 ± 0.11 |
| Snowfield | 31 | 2.28 | -26.63 ± 14.14 | -11.67 ± 6.19 | -0.21 ± 0.11 |
| 1975 | 25 | 8.09 | -143.32 ± 50.91 | -17.71 ± 6.29 | -0.43 ± 0.15 |
| Glacier | 9 | 7.44 | -137.50 ± 46.93 | -18.48 ± 6.31 | -0.45 ± 0.15 |
| Snowfield | 16 | 0.65 | -5.83 ± 3.98 | -8.97 ± 6.13 | -0.22 ± 0.15 |
| **Sierra Nevada** | | | | | |
| 1975 | 16 | 0.39 | -4.19 ± 2.38 | -10.74 ± 6.09 | -0.26 ± 0.15 |
| Glacier | 2 | 0.13 | -1.85 ± 0.73 | -14.57 ± 5.73 | -0.36 ± 0.14 |
| Snowfield | 14 | 0.26 | -2.35 ± 1.65 | -8.90 ± 6.26 | -0.22 ± 0.15 |
| 1980 | 35 | 2.61 | -42.98 ± 18.44 | -16.44 ± 7.05 | -0.46 ± 0.20 |
| Glacier | 12 | 1.95 | -34.69 ± 13.74 | -17.76 ± 7.04 | -0.49 ± 0.20 |
| Snowfield | 23 | 0.66 | -8.30 ± 4.70 | -12.55 ± 7.10 | -0.35 ± 0.20 |
| 1985 | 109 | 3.87 | -40.62 ± 18.78 | -10.50 ± 4.86 | -0.34 ± 0.16 |
| Glacier | 9 | 1.40 | -19.27 ± 8.63 | -13.79 ± 6.18 | -0.44 ± 0.20 |
| Snowfield | 100 | 2.47 | -21.35 ± 10.15 | -8.64 ± 4.11 | -0.28 ± 0.13 |
| **Wind River** | | | | | |
| 1970 | 64 | 23.95 | -365.80 ± 115.43 | -15.28 ± 4.82 | -0.33 ± 0.10 |
| Glacier | 19 | 21.17 | -345.41 ± 102.55 | -16.31 ± 4.84 | -0.35 ± 0.11 |
| Snowfield | 45 | 2.77 | -20.40 ± 12.89 | -7.35 ± 4.64 | -0.16 ± 0.10 |

| | | | | | | |
|---|---|---|---|---|---|---|
| 1975 | 24 | 0.60 | -3.61 ± | 2.82 | -6.01 ± 4.70 | -0.15 ± 0.11 |
| Glacier | 1 | 0.05 | -1.12 ± | 0.27 | -20.90 ± 4.96 | -0.51 ± 0.12 |
| Snowfield | 23 | 0.55 | -2.49 ± | 2.56 | -4.55 ± 4.68 | -0.11 ± 0.11 |